2024 IEEE/RSJ International Conference on Intelligent Robots and Systems (IROS)
October 14-18, 2024. Abu Dhabi, UAE

Adaptive Smith Predictor Fractional Control of a Tele-operated Flexible Link Robot*

Saddam Gharab[1], Selma Benftima[2] and Vicente Feliu Batlle[3]

Abstract— **This work addresses the adaptive Smith predictor control of a tele-operated robot composed of a flexible link. Measurements of the angle of the motor that moves the arm by using an encoder and the moment at the base of the arm by using two strain gauges are fed back. These strain gauges normally present noticeable offset and high-frequency noise. In order to implement such control, the simultaneous real-time characterizations of the main vibration mode - which changes with the carried payload - and the delay of the tele-operated robot - which is time-varying - are carried out using a new algorithm based on an algebraic identification technique, which is robust to the previous strain gauge disturbances. This algorithm is faster than others previously developed, being especially suited to implement an adaptive version of the Smith predictor. The control of the tip position of the robot is closed using a fractional order controller, which has the advantage of removing the steady state error introduced by the strain gauges offset on the tip position. This adaptive control system is subsequently evaluated on a prototype. Simulated and experimental results are presented demonstrating the speed, accuracy, and robustness of the performed control system.**

I. INTRODUCTION

Tele-operated robots perform tasks in environments that can be dangerous for humans. These robotic systems are designed to be remotely controlled by a human operator. In teleoperation, an operator controls the movements and actions of the robot from a remote location through a control interface that sends commands. Tele-operated Flexible Link Robots ($TFLRs$) are robots constructed with lightweight materials, allowing them to be easily transported, navigate sophisticated spaces, consume less energy, and, compared to rigid teleoperated robots, facilitate their mounting on other platforms. $TFLRs$ are used in various applications, primarily in the aerospace industry [1] where they perform tasks in hazardous environments, as well as in the surgical medical domain [2],[3], allowing surgeons to perform surgeries remotely. However, controlling $TFLR$s presents several challenges: (1) the delay in communication between the operator and the robot, known as latency, can have significant implications during the robot's operation, and (2) vibrations due to the flexibility of the links can significantly decrease the positioning accuracy of the robot's end effector and may cause damage to the mechanical system if their natural frequencies are not correctly identified and the control system is not adjusted accordingly. The delay can vary over time due to the different operational states of the communication lines, and the natural vibration frequencies also change over time depending on the mass of the load that the robot is transporting. Additionally, it should be noted that the sensors typically used to measure and provide feedback on the vibrations - pairs of strain gauges located at the base of each link - usually have an offset that varies over time, along with high-frequency noise. It is worth mentioning that the other sensors, which are encoders measuring the rotation of the shaft of each motor, do not encounter these issues. Therefore, robust real-time identification techniques are required to ensure rapid estimations of the characteristic parameters of $TFLR$ dynamics, particularly the vibration modes of the mechanical system and the delay, to implement adaptive controls that reduce the controlled robot's sensitivity to the aforementioned variations. There are many methods for carrying out parametric identification of vibration modes, such as adaptive notch filtering [4], Kalman filtering [5], and least squares methods [6]. Similarly, for identifying delays present in tele-operated systems, estimators have been developed, such as the super-twisting adaptive algorithm [7], spectral formulation [8], or the use of cross-convolution equations [9]. However, these algorithms require the establishment of initial parameter values that influence the method's efficiency and demand proper selection of other parameters, leading to increased computational complexity. They also require several cycles to converge to appropriate vibration frequency values and are relatively sensitive to noise. A relatively recent approach is algebraic framework-based estimators and compared to other classical method of estimation [10]. These were originally proposed in [11] and have been used to design algorithms that estimate real-time oscillations of a noisy signal in cases such as a vibration frequency [12], vibration with slight damping [13], vibration with sensor offset [14], and two vibration modes of an elastic beam from offset-free measurements of a single signal [15]. These estimators offer the advantages of providing very rapid estimation of the parameters of interest, being relatively simple, and not requiring initial states or initial parameter adjustments. Several control strategies of teleoperated robots were reported in the literature in order to accommodate challenges in robots. A study focusing on using Yaskawa robots with the Robot Operating System (*ROS*) for tele-operation tasks is presented in [16]. The work proposed a standard *ROS*-based control by incorporating a new velocity control mode into the standard Motoman *ROS* driver in

*This work was not supported by any organization

[1]Saddam Gharab and Selma Benftima are Researchers with Instituto de Investigaciones Energéticas y Aplicaciones Industriales, Universidad de Castilla La Mancha, 13005, Ciudad Real, Spain saddam.gharab@uclm.es

[2]Vicente Feliu Batlle is Researcher with Escuela Técnica Superior De Ingenieros Industriales, Universidad de Castilla La Mancha, Avenida Camilo José Cela, 13001, Ciudad Real, Spain vicente.feliu@uclm.es

order to accommodate trajectory tracking errors and time delay. The designed control method is validated by applying it to the Yaskawa GP8 robot. A local Partial Feedback Linearization control technique was proposed in [17], based on a modified Extended Lawrence Four-Channel architecture to ensure stability and good monitoring of flexible slave arms in a master-slave telerobotic system. The stability criteria for the varying delay was generalized and the designed control was applied to lightweight cable-driven tools in telerobotic surgery. A controller based on *PD* structure was developed in [18] combined with a disturbance observer to compensate for dynamic uncertainties, disturbances, time delay, and actuator failures in a teleoperation system where the slave arm is flexible. The stability of the designed controller was verified using the Lyapunov theory. Two controllers are introduced in [19]: an adaptive and damping injection controller that addresses uncertainties in plant parameters, and a proportional plus damping injection controller that regulates a nonlinear teleoperated manipulator with joint flexibility and time-delays. The adaptive controller can handle parameter uncertainties and constant time delays, while the other controller is robust to variable time delays and both controllers can achieve good position tracking. The key contributions of this work include (1) The design of new algebraic estimators for rapidly identifying the parameters of the $TFLR$, (2) The development of an adaptive predictive fractional order controller based on a PD structure and a Smith predictor. This control scheme is validated on a 1-*DOF* flexible manipulator. Additionally, the parameters of the controller, such as the time delay and natural frequency, are auto-tuned using online algebraic estimators. The article has been structured as follows. Section *II* presents an overview of the experimental setup and the dynamic model of the system. Section *III* develops two real-time rapid algebraic identifiers that estimate the vibration frequency, stiffness, gain of the motor loop, and delay of the dynamic model. The designed estimator is applied in Section *IV* to monitor the vibrations of an experimental $TFLR$ with one degree of freedom, and the results obtained in experimentation are presented. Section *V* deals with the control scheme adapted to monitor the teleoperated manipulator in order to ensure trajectory tracking and eliminate vibrations. Finally, conclusions are drawn in the last section.

II. Dynamic Model of the $TFLR$

A. Description of the experimental platform

The air table flexible manipulator of Fig. 1 is a precision mechanism designed for agile and controlled movements in various applications. It consists of three metallic legs forming a stable base on which a *DC* servo motor with a reduction ratio of $n = 25$ is installed. This motor serves as the primary driving force for the manipulator's motion. A 0.5 m long flexible arm is attached to the servo motor. This arm is capable of bending and flexing to accommodate different trajectories and reach desired positions accurately. At the end of the manipulator arm, a disc system with a radius of 6 *cm* is mounted. The entire system operates on an air table, which effectively reduces friction and ensures smooth movements of the manipulator. This feature is crucial for maintaining precision and accuracy in positioning tasks.

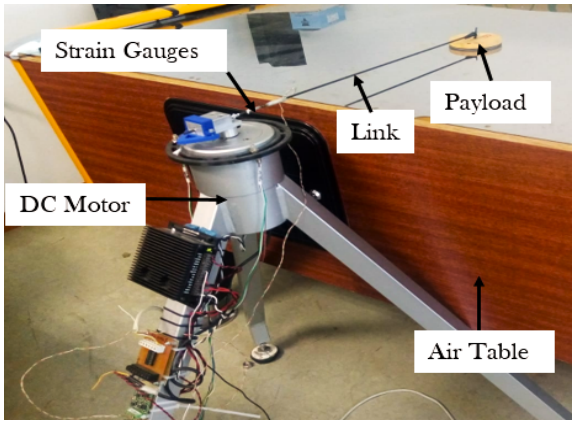

Fig. 1. Air Table Flexible Robot System.

B. Dynamics of the Complete System

Consider the one degree of freedom $TFLR$ of Fig. 1, in which the angular position of the motor that moves the link is $\theta_m(rad)$, the coupling torque measured at the base of the link by a pair of strain gauges is $\Gamma(N \cdot m)$, and the tip angle is $\theta_t(rad)$. Taking into account the length and the stiffness of the link, and the tip mass (see Table I), only the fundamental frequency is excited when carrying out a horizontal movement of the set (motor + link). The rest of the modes can be neglected because they have frequencies much higher than the first one and amplitudes much smaller. Then the following model of our $TFLR$ is proposed:

$$m \cdot l^2 \cdot \ddot{\theta}_t(t) = k \cdot (\theta_m(t) - \theta_t(t)) = \Gamma(t) \tag{1}$$

where m is the mass of the tip payload, l is the length of the link, and k is the stiffness coefficient of the robot link given by the expression $k = \frac{3 \cdot EI}{l}$ where EI is the flexural stiffness. The dynamics of the *DC* motor is:

$$K \cdot u(t) = J \cdot \ddot{\theta}_m(t) + \nu \cdot \dot{\theta}_m(t) + \Gamma_c(t) + \Gamma(t) \tag{2}$$

where K is the electromechanical constant, u is the voltage applied to the motor, J is the motor's inertia, ν is the viscous friction, and Γ_c is the Coulomb friction. The values of the physical parameters of the motor and the flexible mechanism are shown in Table I.

Our setup is equipped with a sensory system comprising an incremental encoder embedded into the *DC* motor, enabling precise determination of the motor's angular position with an accuracy of $7 \cdot 10^{-5}$ *rad*. Additionally, a pair of strain gauges, with a gauge factor of 2.16 and resistance of 120.2 Ω, is positioned at the base of the link. Typically, robot actuators consist of servo systems integrated with controllers that regulate joint positions, minimizing the impact of viscous and Coulomb frictions. Our platform's motor is governed by a 2-*DOF PID* controller, designed based on the dynamics described in (2), leading to a critically damped second-order closed-loop system. The delay associated with the operator

TABLE I

VALUES AND UNITS OF ROBOT PROPERTIES.

Property	Value	Unit
Mass of the payload (m)	[0.05]	[Kg]
Length of the link (l)	[0.65]	[m]
Stiffness of the link (k)	[0.56]	[$N \cdot m^{-1}$]
Inertia of the motor (J)	[$6.87 \cdot 10^{-5}$]	[$kg \cdot m^2$]
Viscous friction (ν)	[$1.041 \cdot 10^{-3}$]	[$N \cdot m \cdot s$]
Coulomb friction constant (Γ_c)	[$119.7 \cdot 10^{-3}$]	[$N \cdot m$]
Electromechanical constant (K)	[0.21]	[$N \cdot m.V^{-1}$]
Flexural stiffness (EI)	[0.260]	[$N \cdot m^2$]
Sampling time (Ts)	[2]	[ms]

communication is denoted by τ and incorporated after the set-point θ_m^*. This set point manipulated by the operator, after having been delayed, serves as the reference for the motor's control loop. The resulting dynamics' transfer function is represented by equation (3), where $M(s)$ is the transfer function of the motor's controlled dynamics, and μ stands for the inverse of the modulus of the double pole tailored for the closed loop.

$$\frac{\theta_m(s)}{\theta_m^*(s)} = M(s) \cdot e^{-\tau \cdot s} \quad , \quad M(s) = \frac{1}{(1+\mu \cdot s)^2} \tag{3}$$

Moreover, taking Laplace transforms in (1) and operating, it is obtained that

$$G_\Gamma(s) = \frac{\Gamma(s)}{\theta_m(s)} = \frac{k \cdot s^2}{s^2 + \varpi^2} \quad , \quad G_\theta(s) = \frac{\theta_t(s)}{\theta_m(s)} = \frac{\varpi^2}{s^2 + \varpi^2} \tag{4}$$

Fig. 2a shows the experimental step response of the arm tip, θ_t, and Fig. 2b shows the magnitude of the frequency response of the signal provided by the strain gauges. They show that: 1) the assumption that only the fundamental frequency is excited is true and 2) the dynamics of our robot are accurately described by equations (1), (3).

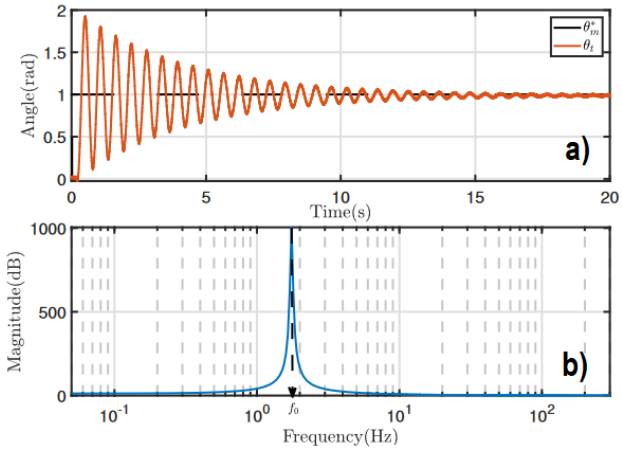

Fig. 2. Time and Frequency Responses.

III. DEVELOPMENT OF THE ALGEBRAIC ESTIMATOR

In this section, a novel estimation algorithm is developed based on the principles of algebraic identification, utilizing the dynamic model (1), (3) of the teleoperated flexible robot. It is important to note that the algebraic estimator does not possess asymptotic properties and does not necessitate statistical knowledge of signal noise. Another significant advantage is its ability to rapidly estimate parameters using just the measured input and output variables. This makes it highly suitable for adaptive controller tuning. Fig. 3 illustrates a schematic diagram including two parameter identification processes. Two algebraic estimators are employed: the first one identifies the delay τ and the parameter μ from the reference signal θ_m^* and the motor angle θ_m. Meanwhile, the second one determines the vibration frequency ϖ and the link stiffness k from the motor angle θ_m and the coupling torque Γ.

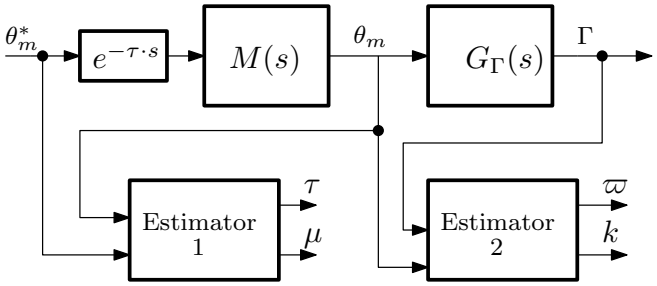

Fig. 3. Diagram of the Algebraic Estimator.

The proposed technique does not require initial conditions (which are unknown) and generates linear relationships between the unknown parameters, enabling rapid convergence towards the actual values of the system parameters.

A. Estimator 1

Applying the first-order Padé approximation to the delay term of $M(s) \cdot e^{-\tau \cdot s}$ of expressions (3) we obtain:

$$\theta_m(s) \cdot (1+\mu \cdot s)^2 \cdot (1+\frac{\tau}{2} \cdot s) = (1-\frac{\tau}{2} \cdot s) \cdot \ \theta_m^*(s) \tag{5}$$

Differentiating three times with respect to s we get:

$$\tau \cdot \mu^2 \cdot \left(3 \cdot \theta_m(s) + 6 \cdot s \cdot \frac{d\theta_m(s)}{ds} + 3 \cdot s^2 \cdot \frac{d^2\theta_m(s)}{ds^2} + \frac{1}{2} \cdot s^3 \cdot \frac{d^3\theta_m(s)}{ds^3}\right) +$$
$$\mu^2 \cdot \left(6 \cdot \frac{d\theta_m(s)}{ds} + 6 \cdot s \cdot \frac{d^2\theta_m(s)}{ds^2} + s^2 \cdot \frac{d^3\theta_m(s)}{ds^3}\right) + \mu \cdot (6 \cdot \frac{d^2\theta_m(s)}{ds^2} +$$
$$2 \cdot s \cdot \frac{d^3\theta_m(s)}{ds^3}) + \mu \cdot \tau \cdot \left(6 \cdot \frac{d\theta_m(s)}{ds} - 6 \cdot s \cdot \frac{d^2\theta_m(s)}{ds^2} + s^2 \cdot \frac{d^3\theta_m(s)}{ds^3}\right) +$$
$$\tau \cdot \left(\frac{1}{2} \cdot s \cdot \frac{d^3\theta_m(s)}{ds^3} + \frac{1}{2} \cdot s \cdot \frac{d^3\theta_m^*(s)}{ds^3} + \frac{3}{2} \cdot \frac{d^2\theta_m(s)}{ds^2} + \frac{3}{2} \cdot \frac{d^2\theta_m^*(s)}{ds^2}\right) =$$
$$-\frac{d^3\theta_m(s)}{ds^3} + \frac{d^3\theta_m^*(s)}{ds^3} \tag{6}$$

In order to avoid multiplications by positive powers of s, which result in unwanted time derivatives, equation (6) is multiplied by s^{-3}:

$$\tau\cdot\mu^2\cdot(3\cdot s^{-3}\cdot\theta_m(s)+6\cdot s^{-2}\cdot\frac{d\theta_m(s)}{ds}+3\cdot s^{-1}\cdot\frac{d^2\theta_m(s)}{ds^2}+\frac{1}{2}\cdot\frac{d^3\theta_m(s)}{ds^3})+\mu^2\cdot(6\cdot s^{-3}\cdot\frac{d\theta_m(s)}{ds}+6\cdot s^{-2}\cdot\frac{d^2\theta_m(s)}{ds^2}+s^{-1}\cdot\frac{d^3\theta_m(s)}{ds^3})+\mu\cdot(6\cdot s^{-3}\cdot\frac{d^2\theta_m(s)}{ds^2}+2\cdot s^{-2}\cdot\frac{d^3\theta_m(s)}{ds^3})+\mu\cdot\tau\cdot(6\cdot s^{-3}\cdot\frac{d\theta_m(s)}{ds}-6\cdot s^{-2}\cdot\frac{d^2\theta_m(s)}{ds^2}+s^{-1}\cdot\frac{d^3\theta_m(s)}{ds^3})+\tau\cdot(\frac{1}{2}\cdot s^{-2}\cdot\frac{d^3\theta_m(s)}{ds^3}+\frac{1}{2}\cdot s^{-2}\cdot\frac{d^3\theta_m^*(s)}{ds^3}+\frac{3}{2}\cdot s^{-3}\cdot\frac{d^2\theta_m(s)}{ds^2}+s^{-3}\cdot\frac{3}{2}\cdot\frac{d^2\theta_m^*(s)}{ds^2})=-s^{-3}\cdot\frac{d^3\theta_m(s)}{ds^3}+s^{-3}\cdot\frac{d^3\theta_m^*(s)}{ds^3} \tag{7}$$

In order to translate equation (7) into the time domain, the inverse Laplace transform, denoted hereafter as $\mathscr{L}^{-1}$, is carried out. Recall the following properties: $\mathscr{L}^{-1}s(*)=\frac{d}{dt}(*)$; $\mathscr{L}^{-1}\frac{1}{s}(*)=\int_0^t(*)d\psi$; $\mathscr{L}^{-1}\frac{d^v}{ds^v}()=(-1)^v t^v()$. Moreover, let the operator $\int_0^{(p)}(*)$ represent the integration p times of a function. Taking all this into account, equation (7) is converted to the time domain and can be expressed in a compact form as:

$$\tau\cdot\mu^2\cdot\alpha_1(t)+\mu^2\cdot\beta_1(t)+\mu\cdot\gamma_1(t)+\mu\cdot\tau\cdot\delta_1(t)+\tau\cdot\lambda_1(t)=\sigma_1(t) \tag{8}$$

where $\alpha_1=3\int_0^{(3)}\theta_m(t)+6\int_0^{(2)}t\theta_m(t)+3\int_0^{(1)}t^2\theta_m(t)+\frac{1}{2}\cdot t^3\theta_m(t)$, $\beta_1=6\int_0^{(3)}t\theta_m(t)+6\int_0^{(2)}t^2\theta_m(t)+\int_0^{(1)}t^3\theta_m(t)$, $\gamma_1=6\int_0^{(3)}t^2\theta_m(t)+2\int_0^{(2)}t^3\theta_m(t)$, $\delta_1=6\int_0^{(3)}t\theta_m(t)-6\cdot\int_0^{(2)}t^2\theta_m(t)-\int_0^{(1)}t^3\theta_m(t)$, $\lambda_1=\frac{1}{2}\int_0^{(2)}t^3\theta_m(t)+\frac{1}{2}\int_0^{(2)}t^3\theta_m^*(t)+\frac{3}{2}\int_0^{(3)}t^2\theta_m(t)+\int_0^{(3)}\frac{3}{2}t^2\theta_m^*(t)$,$\sigma_1=-\int_0^{(3)}t^3\theta_m(t)+\int_0^{(3)}t^3\theta_m^*(t)$ and $\alpha_1,\beta_1,\gamma_1,\delta_1,\lambda_1$, and σ_1 are the outputs of the following linear time-varying unstable filters with zero initial states:

$$\begin{array}{lll}
\alpha_1=z_1-\frac{1}{2}\cdot t^3\cdot\theta_m & \beta_1=z_4 & \gamma_1=z_7\\
\dot{z_1}=z_2+3\cdot t^2\cdot\theta_m & \dot{z_4}=-t^3\cdot\theta_m+z_5 & \dot{z_7}=z_8\\
\dot{z_2}=z_3-6\cdot t\cdot\theta_m & \dot{z_5}=6\cdot t^2\cdot\theta_m+z_6 & \dot{z_8}=z_9-2\cdot t^3\cdot\theta_m\\
\dot{z_3}=3\cdot\theta_m & \dot{z_6}=-6\cdot t\cdot\theta_m & \dot{z_9}=6\cdot t^2\cdot\theta_m\\
*** & *** & ***\\
\delta_1=z_{10} & \lambda_1=z_{13} & \sigma_1=z_{16}\\
\dot{z_{10}}=z_{11}-t^3\cdot\theta_m & \dot{z_{13}}=z_{14} & \dot{z_{16}}=z_{17}\\
\dot{z_{11}}=z_{12}-6\cdot t^2\cdot\theta_m & \dot{z_{14}}=-\frac{1}{2}\cdot t^3(\theta_m^*+\theta_m)+z_{15} & \dot{z_{17}}=z_{18}\\
\dot{z_{12}}=-6\cdot t\cdot\theta_m & \dot{z_{15}}=\frac{3}{2}\cdot t^2(\theta_m^*+\theta_m) & \dot{z_{18}}=t^3\cdot(\theta_m-\theta_m^*)
\end{array} \tag{9}$$

The linear equation (8) has five unknown parameters, μ, τ, and their combinations, which can be obtained through a least squares error fit within the time window [t_i,t_f], representing the time interval between the first and last available samples. The cost function to minimize is:

$$\varepsilon_1=\int_{t_i}^{t_f}([\alpha_1(t)\ \ \beta_1(t)\ \ \gamma_1(t)\ \ \delta_1(t)\ \ \lambda_1(t)]\cdot\mathbf{P}^T-\sigma_1(t))^2\cdot dt \tag{10}$$

where $(^T)$ denotes matrix transposition and

$$\mathbf{P}=[\tau\cdot\mu^2\ \ \mu^2\ \ \mu\ \ \mu\cdot\tau\ \ \tau] \tag{11}$$

The minimum ε_1 corresponds to an optimum $\mathbf{P}^*$ given by

$$\mathbf{P}^*=\left[\int_{t_i}^{t_f}\begin{bmatrix}\alpha_1(t)\\ \beta_1(t)\\ \gamma_1(t)\\ \delta_1(t)\\ \lambda_1(t)\end{bmatrix}\cdot\begin{bmatrix}\alpha_1(t)\\ \beta_1(t)\\ \gamma_1(t)\\ \delta_1(t)\\ \lambda_1(t)\end{bmatrix}^T dt\right]^{-1}\cdot\int_{t_i}^{t_f}\begin{bmatrix}\alpha_1(t)\\ \beta_1(t)\\ \gamma_1(t)\\ \delta_1(t)\\ \lambda_1(t)\end{bmatrix}\cdot\sigma_1(t)\,dt \tag{12}$$

Then the parameters τ, μ have to be estimated from the five conditions obtained: $p_1^*=\tau\cdot\mu^2$, $p_2^*=\mu^2$, $p_3^*=\mu$, $p_4^*=\tau\cdot\mu$ and $p_5^*=\tau$ being p_i^*, $i=1\ldots5$ the elements of vector $\mathbf{P}^*$. This is carried out minimizing the quadratic cost function $\underset{\tau_o,\mu_o}{min}\,\Xi$ with $\Xi=(\tau_o\cdot\mu_o^2-\tau\cdot\mu^2)^2+(\mu_o^2-\mu^2)^2+(\mu_o\cdot\tau_o-\mu\cdot\tau)^2+(\mu_o-\mu)^2+(\tau_o-\tau)^2$, which yields the optimum estimates τ_o and μ_o.

B. Estimator 2

As mentioned previously, the strain gauge sensor utilized in the system exhibits an inherent offset, which necessitates careful consideration when developing the estimator. This offset, often a result of manufacturing imperfections or inherent characteristics of the sensor, introduces a baseline deviation in the sensor's output readings. Therefore, the Laplace transform of the measured coupling torque $\hat{\Gamma}$ is

$$\hat{\Gamma}(s)=\Gamma(s)+\frac{\chi}{s} \tag{13}$$

where Γ is the actual value and χ is the offset value. Introducing (13) into the dynamics described by $G_\Gamma(s)$ in the left side of equation (4), we obtain

$$\left(s^3+s\cdot\varpi^2\right)\cdot\hat{\Gamma}(s)-k\cdot s^3\cdot\theta_m(s)-\chi\cdot\left(s^2+\varpi^2\right)=0 \tag{14}$$

Differentiating three times with respect to s we get:

$$\varpi^2\cdot\left(3\cdot\frac{d^2\hat{\Gamma}(s)}{ds^2}+s\cdot\frac{d^3\hat{\Gamma}(s)}{ds^3}\right)-k\cdot\left(6\cdot\theta_m(s)+18\cdot s\cdot\frac{d\theta_m(s)}{ds}+9\cdot s^2\cdot\frac{d^2\theta_m(s)}{ds^2}+s^3\cdot\frac{d^3\theta_m(s)}{ds^3}\right)+\left(6\cdot\hat{\Gamma}(s)+18\cdot s\cdot\frac{d\hat{\Gamma}(s)}{ds}+9\cdot s^2\cdot\frac{d^2\hat{\Gamma}(s)}{ds^2}+s^3\cdot\frac{d^3\theta_m(s)}{ds^3}\right)=0 \tag{15}$$

In order to avoid multiplications by positive powers of s, which result in unwanted time derivatives, we multiply equation (15) by s^{-3}, resulting in:

$$\varpi^2\cdot\left(3\cdot s^{-3}\cdot\frac{d^2\hat{\Gamma}(s)}{ds^2}+s^{-2}\cdot\frac{d^3\hat{\Gamma}(s)}{ds^3}\right)-k\cdot(6\cdot s^{-3}\cdot\theta_m(s)+18\cdot s^{-2}\cdot\frac{d\theta_m(s)}{ds}+9\cdot s^{-1}\cdot\frac{d^2\theta_m(s)}{ds^2}+\frac{d^3\theta_m(s)}{ds^3})+\left(6\cdot s^{-3}\cdot\hat{\Gamma}(s)+18\cdot s^{-2}\cdot\frac{d\hat{\Gamma}(s)}{ds}+9\cdot s^{-1}\cdot\frac{d^2\hat{\Gamma}(s)}{ds^2}+\frac{d^3\hat{\Gamma}(s)}{ds^3}\right)=0 \tag{16}$$

This equation can be translated into the time domain:

$$\varpi^2 \cdot \left(3 \cdot t^2 \cdot \int_0^{(3)} \hat{\Gamma}(t) - t^3 \cdot \int_0^{(2)} \hat{\Gamma}(t)\right) -$$
$$k \cdot (6 \cdot \int_0^{(3)} \theta_m(t) - 18 \cdot \int_0^{(2)} t \cdot \theta_m(t) + 9 \cdot t^2 \cdot \int_0^{(1)} \theta_m(t) + t^3 \cdot \theta_m(t)) +$$
$$(6 \cdot t^3 \cdot \int_0^{(3)} \hat{\Gamma}(t) - 18 \cdot t \cdot \int_0^{(1)} \hat{\Gamma}(t) + 9 \cdot t^2 \cdot \int_0^{(1)} \hat{\Gamma}(t) + t^3 \cdot \hat{\Gamma}(t)) = 0 \tag{17}$$

and written in a compact form as:

$$\varpi^2 \cdot \alpha_2(t) + k \cdot \beta_2(t) = \gamma_2(t) \tag{18}$$

where α_2, β_2, and γ_2 are the outputs of the following time-varying linear unstable filters with zero initial states:

$$\begin{array}{lll} \alpha_2 = z_1 & \beta_2 = t^3 \cdot \theta_m + z_4 & \gamma_2 = t^3 \cdot \hat{\Gamma} + z_7 \\ \dot{z}_1 = z_2 & \dot{z}_4 = 9 \cdot t^2 \cdot \theta_m + z_5 & \dot{z}_7 = 9 \cdot t^2 \cdot \hat{\Gamma} + z_8 \\ \dot{z}_2 = -t^3 \cdot \hat{\Gamma} + z_3 & \dot{z}_5 = -18 \cdot t \cdot \theta_m + z_6 & \dot{z}_8 = -18 \cdot t \cdot \hat{\Gamma} + z_9 \\ \dot{z}_3 = 3 \cdot t^2 \cdot \hat{\Gamma} & \dot{z}_6 = 6 \cdot \theta_m & \dot{z}_9 = 6 \cdot \hat{\Gamma} \end{array} \tag{19}$$

The linear equation (18) has two unknown parameters, ϖ^2 and k, which can be obtained through a least squares error fit within the time window $[t_i, t_f]$, representing the time interval between the first and last available samples. The cost function to minimize is:

$$\varepsilon_2 = \int_{t_i}^{t_f} \left([\alpha_2(t) \quad \beta_2(t)] \cdot [\varpi^2 \quad k]^T - \gamma_2(t)\right)^2 \cdot dt \tag{20}$$

In order to estimate ϖ^2 and k, minimizing ε_2 leads to:

$$\begin{bmatrix} \varpi^2 \\ k \end{bmatrix} = \left[\int_{t_i}^{t_f} \begin{bmatrix} \alpha_2(t) \\ \beta_2(t) \end{bmatrix} \cdot \begin{bmatrix} \alpha_2(t) \\ \beta_2(t) \end{bmatrix}^T dt\right]^{-1} \int_{t_i}^{t_f} \begin{bmatrix} \alpha_2(t) \\ \beta_2(t) \end{bmatrix} \gamma_2(t)\, dt \tag{21}$$

C. Sentinel Algorithm

Since filters (9) and (19) are unstable, expressions (12) and (21) involve divisions of very high magnitudes when the elapsed time is long. Then numerical errors are produced in these divisions that yield incorrect estimations of the system parameters. Then it is essential to employ sentinel algorithms that stop the identification process when the parameters have been accurately estimated, preventing the errors produced if the algorithms were run for a long time. Moreover, these sentinels ensure the accurate selection of the estimated parameters, are indicators of the estimation accuracy, and determine when the identification process should cease and the parameters of the adaptive controller should be retuned.

The sentinel algorithm employed here is based on the Exponentially Weighted Moving Average (*EWMA*) and Exponentially Weighted Moving Standard Deviation (*EWMSTD*). The recursive formulae of the *EWMA* and the *EWMSTD* are respectively $Z(j) = \lambda_1 \cdot X(j) + (1-\lambda_1) \cdot Z(j-1)$ and $S(j) = \sqrt{\lambda_2 \cdot (X(j) - Z(j))^2 + (1-\lambda_2) \cdot S^2(j-1)}$, where X represents any of the parameters to be estimated, $0 < \lambda_{1,2} \leq 1$ are the forgetting factors that handle the smoothness of the trajectory and j is the sampling index. It is important to note that the initialization values for the *EWMA* and the *EWMSTD* are defined as $Z(1) = X(1)$ and $S(1) = X(1)$. By using these definitions and the outputs of the algebraic estimator, it is considered that the estimates have converged when the following condition is fulfilled:

$$\frac{S(j)}{|Z(j)|} \leq \delta \tag{22}$$

where δ is a chosen precision threshold.

IV. Application of the Estimator

The above estimators are applied to a simulated model of the *TFLR* and are implemented into the program of the considered robot. Fig. 4 shows the measured signals, which serve as inputs to the estimators and are utilized for identifying the parameters as indicated in Fig. 3. However, only estimations of ϖ and τ will be presented, as these parameters are the most critical for control purposes.

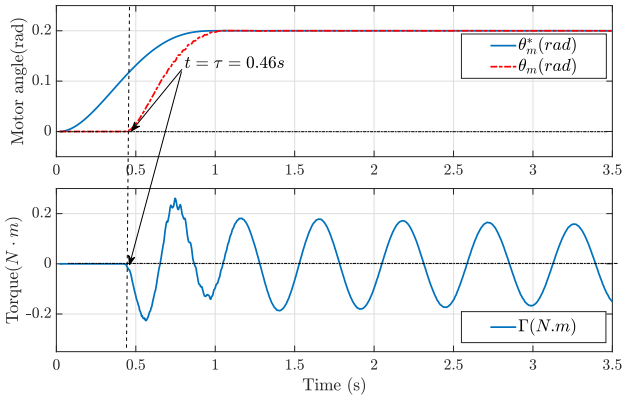

Fig. 4. Experimental Signals Used for the Algebraic Estimation.

The natural frequency is employed in designing the *TFLR* control system, serving as crucial data for efficiently canceling vibrations. Its real value ϖ_r is determined via Fast Fourier Transform (*FFT*) and stands at 11.52 $rad.s^{-1}$. Estimator 2 yields a suitable value of around 11.518 $rad.s^{-1}$ in less than 0.65 s with a relative error of 0.017%. Knowing the delay enables implementing compensatory measures to synchronize the robot's behavior with the desired motion or trajectory. It also allows for achieving precise control and enhancing the dynamics in closed-loop systems. The system's real delay is τ_r= 0.46 s and Estimator 1 is capable of providing the exact value in less than 0.2 seconds. The evolution of the estimated frequency and delay, and their real values, are illustrated in Fig. 5.

The sentinels, determined by the convergence criterion (22), are depicted in Fig. 6 for both estimated frequency and delay. This illustrates that acceptable estimated values for frequency and delay can be chosen, starting from 0.65 s and 0.15 s, respectively. The proposed algebraic estimator involves two phases: the estimation procedure and the convergence criterion. The two algebraic estimators established previously will be employed to auto-tune the parameters of a designed Smith predictor fractional order controller, applied

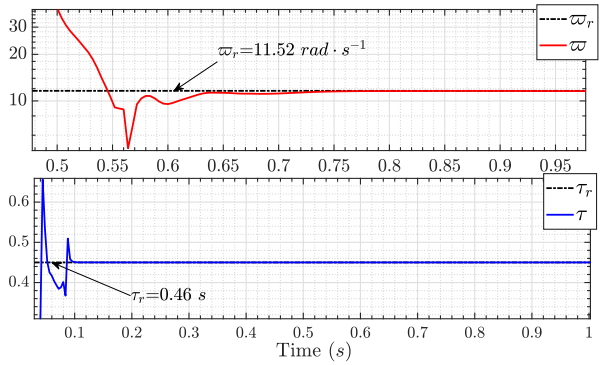

Fig. 5. Experimental Evolution and Convergence of the Natural Frequency and the Time Delay Obtained in Real Time with Respectively Estimator 2 and 1.

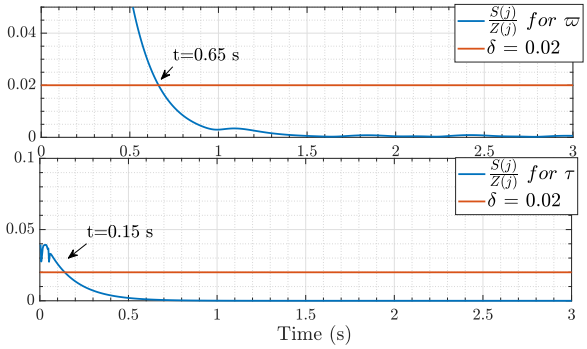

Fig. 6. Evolution of the Sentinels.

to the 1-*DOF* flexible robot presented in Section *II*. The rapid estimation of *TFLR* parameters enhances the suitability of the designed controller.

V. Adaptive Fractional-order Derivative Controller Embedded in a Smith Predictor Structure

We consider the Smith predictor-based control scheme depicted in Fig. 7, wherein $M(s)$ denotes the real equivalent transfer function of the controlled servo motor. Specifically, we define $M(s) = \frac{1}{(1+\mu \cdot s)^2}$, with $\mu = 0.02$. The motor is regulated using a robust 2-*DOF PID* controller, with its double pole located at $p = -\frac{1}{\mu}$. This placement renders the motor dynamics robust against variations in mechanical vibration of the beam and friction (either Coulomb or dynamic frictions). Furthermore, the motor dynamics exhibit a response significantly faster than the mechanical vibration of the beam. Here, $G_\theta(s)$ characterizes the real relationship between the tip position and the motor angle, while τ denotes the real-time delay attributable to data transmission between the control center and the servo-controlled motor. In this figure, $M^*(s)$, $G^*_\theta(s)$ and τ^* represent the model transfer functions of $M(s)$ and $G_\theta(s)$, and the model of τ. Since the motor control is robust, we assume hereafter that $M(s) = M^*(s)$. However, $G_\theta(s)$ varies in function of the carried payload and τ in function on the operational state of the communication line.

The parameters $\varpi^* = 11.518\ rad.s^{-1}$, $\tau^* = 0.46\ s$ are considered as the nominal values of respectively the natural frequency and the delay, and $R(s)$ represents the controller. Accordingly, the values of τ^*, K_d and ϖ are adapted based on the estimation performed by the algebraic estimator.

Equating the right part of equation (1) gives and estimator of the tip position $\theta_t(t)$ of the robot based on measurements of the motor angle $\theta_m(t)$ and the strain gauges $\Gamma(t)$:

$$\theta_t(t) = \theta_m(t) - \frac{\Gamma(t)}{k} \tag{23}$$

Since $\Gamma(t)$ has an offset χ, a constant disturbance $d(t)$ of amplitude $-\frac{\chi}{k}$ is produced in the estimation of $\theta_t(t)$. It is modelled in Fig. 7 as a step disturbance $d(s) = \frac{\bar{d}}{s}$ where $\bar{d} = \frac{-\chi}{k}$.

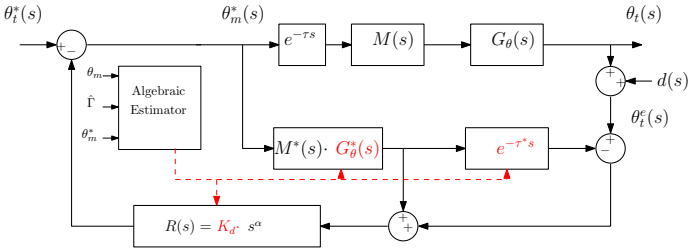

Fig. 7. Feedback Control Scheme.

A. Offset Disturbance Rejection

Operating the block diagram of Fig. 7, the closed-loop transfer functions of this system are obtained:

$$\theta_t(s) = \frac{G_\theta(s)\cdot M(s)\cdot e^{-\tau\cdot s}\cdot((\theta_t^*(s) - R(s)\cdot d(s))}{1+R(s)\cdot M(s)\cdot G^*_\theta(d)+R(s)\cdot M(s)\cdot\left(G_\theta(s)\cdot e^{-\tau\cdot s} - G^*_\theta(s)\cdot e^{-\tau^*\cdot s}\right)} \tag{24}$$

Given the significantly faster dynamics of the motor compared to the vibration of the flexible link, we can reasonably assume that $M(s) = 1$. Accordingly, we get that

$$\theta_t(s) = H_\theta(s)\cdot\theta_t^*(s) + H_d(s)\cdot d(s) \tag{25}$$

where

$$H_\theta(s) = \frac{G_\theta(s)\cdot e^{-\tau\cdot s}}{1+R(s)\cdot G^*_\theta(d)+R(s)\cdot\left(G_\theta(s)\cdot e^{-\tau\cdot s} - G^*_\theta(s)\cdot e^{-\tau^*\cdot s}\right)} \tag{26}$$

$$H_d(s) = -\frac{R(s)\cdot G_\theta(s)\cdot e^{-\tau\cdot s}}{1+R(s)\cdot G^*_\theta(d)+R(s)\cdot\left(G_\theta(s)\cdot e^{-\tau\cdot s} - G^*_\theta(s)\cdot e^{-\tau^*\cdot s}\right)} \tag{27}$$

Applying the Final Value Theorem to these expressions and taking into account that $G_\theta(0) = G^*_\theta(0) = 1$, we get the gain of $H_\theta(s)$ and the steady state error caused by $d(s)$. They are respectively:

$$\lim_{s\to 0} H_\theta(s) = \frac{1}{1+R(0)}\ ,\ \lim_{s\to 0} H_d(s)\cdot\bar{d} = \frac{R(0)}{1+R(0)}\cdot\bar{d} \tag{28}$$

This suggests that, in order to get a unity gain in the closed-loop system and a zero steady-state error to strain gauge offset, it is required that $R(0) = 0$.

B. Control Design: Frequency Domain Based Technique

The previous condition implies that controller $R(s)$ cannot have a proportional term. It must have only a derivative term being its simplest form $R(s) = K_d \cdot s$. This controller has a single parameter to be tuned which means that we will be able to design a single dynamic specification (either in the time or frequency domains). Then we propose to use a fractional-order derivative controller of the form

$$R(s) = K_d \cdot s^{\alpha} \ , \ 0 < \alpha \tag{29}$$

which verifies that $R(0) = 0$ and has two parameters to be tuned (K_d and α) allowing us to design two dynamic specifications. We choose to design the controller in the frequency domain defining a phase margin $\phi_m(rad)$ and a gain crossover frequency $\omega_c(rad \cdot s^{-1})$.

Let us assume that the model $G^*_\theta(s)$, τ^* perfectly matches the real process $G_\theta(s)$, τ. Then transfer function (26) becomes

$$H_\theta(s) = \frac{G_\theta(s) \cdot e^{-\tau \cdot s}}{1 + R(s) \cdot G_\theta(s)} \tag{30}$$

and the open loop frequency response is $L(j \cdot \omega) = R(j \cdot \omega) \cdot G_\theta(j \cdot \omega)$. The condition to design a controller (29) that verifies the previous two specifications is [20]:

$$\frac{\varpi^2}{(j \cdot \omega_c)^2 + \varpi^2} \cdot K_d (j \cdot \omega_c)^{\alpha} = -e^{j \cdot \phi_m} \tag{31}$$

Equating the magnitude and phase of this complex expression and assuming that $\omega_c > \varpi$ yields the rules to tune the fractional-order controller:

$$\alpha = \frac{2 \cdot \phi_m}{\pi} \ , \ K_d = \frac{\omega_c^2 - \varpi^2}{\varpi^2 \cdot \omega_c^{\alpha}} \tag{32}$$

Fig. 8 plots the first path of the Nyquist diagram of $L(j \cdot \omega)$ for $0 < \omega < \infty$. The solid blue line represents $R(s) = 1$ and depicts a marginally stable closed-loop system with a phase margin of $\phi_m = 0$ degrees. To enhance the relative stability by increasing the phase margin, the phase lead controller $R(s)$ is introduced to add a phase margin equal to ϕ_m to the open-loop system. Then the solid red line shows the Nyquist diagram of $L(j\omega)$ using the controller (29) in which the corresponding critical point is represented. This diagram shows that this fractional order differentiator decals the critical point of $G_\theta(j \cdot \omega)$ adding a phase margin equal to $\frac{\alpha \cdot \pi}{2}$. The stability of the closed-loop system is ensured for $\omega_c > \omega_0$ if $\phi_m > 0$ and $\alpha < 2$.

We pursue an overdamped and fast step response of $H_\theta(s)$. Then we choose the frequency specifications $\phi_m = 80^\circ$ and $\omega_c = 12.26 \ rad \cdot s^{-1}$. It is well known that ϕ_m is related to the damping and the chosen value guarantees overdamping, and ω_c is related to the settling time, and the chosen value guarantees reaching the $\pm 5\%$ of the final value in less than $1 + \tau$ s. The first expression of (32) yields $\alpha = 0.89$. The second expression of (32) yields $K_d = 0.0138$ in the case of a nominal payload of $50g$, which implies that $\varpi_0 = 11.54$ $rad \cdot s^{-1}$.

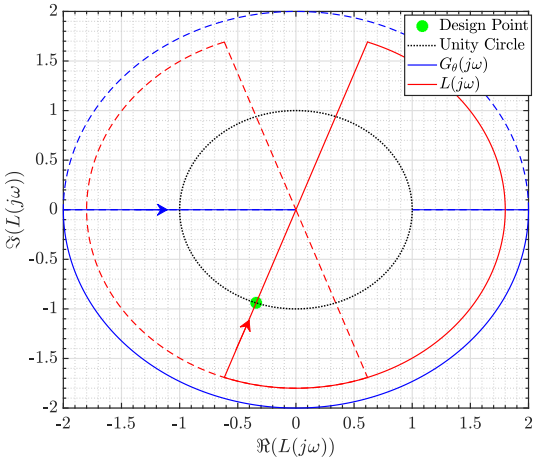

Fig. 8. Control Design Technique Based on Nyquist Plots.

C. Experimental Control System Validation

Experiments are carried out that estimate the time delay and the fundamental vibration frequency in real time. The Smith predictor scheme is combined with the controller (29). Once the two identification processes have estimated the robot parameters, the parameters of the blocks of the controller of Fig. 7 are updated: ϖ^* in $G^*_\theta(s)$, τ^* in the delay block $e^{-\tau^* \cdot s}$, and K_d is calculated in function of the estimated ϖ in $R(s)$. The parameters of the controllers are initially tuned in accordance with the nominal robot parameters: $\varpi_0 = 11.54 \ rad \cdot s^{-1}$ and time delay $\tau_0 = 0.5 \ s$. These controller parameters are maintained from the beginning of the maneuver until they are updated.

Figures 9 and 10 demonstrate that the designed $R(s)$ achieves both guaranteed tracking and offset perturbation rejection simultaneously, in the cases of changes of the tip payload and time delay respectively.

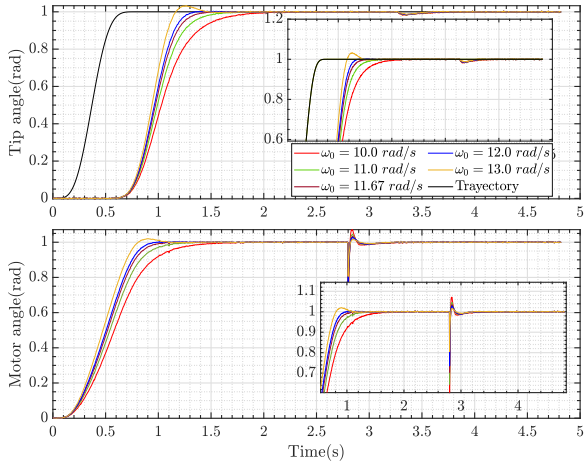

Fig. 9. Experimental Validation of the Adaptive Control Scheme When There is a Change in the Tip Payload m and, Consequently, in the Vibration Frequency ϖ

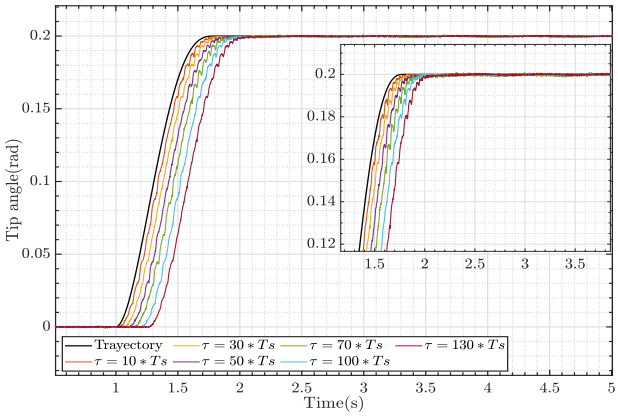

Fig. 10. Experimental Validation of the Adaptive Control Scheme When There is a Change in the Time Delay τ.

VI. CONCLUSIONS

Tele-operated robots with flexible links are of interest in applications such as large space robots, medical surgery and exploration, and large robots for construction and infrastructure maintenance. However, their control is complicated due to simultaneous time-varying delays and vibrations. In this context, the developed estimators are useful as they allow obtaining in real-time the delay and the frequency of the dominant vibration mode of the robot. This information enables the development of adaptive controls that enhance the performance and stability of such robots. The estimators developed in this article are original and are based on the general methodology of algebraic identification, offering several advantages: they provide faster estimation compared to other identification algorithms, do not require any initialization values, and can be relatively insensitive to high-frequency noise, and the offset present in the measurements.

In order to ensure stability and good performance of the manipulator when tracking a desired trajectory while avoiding vibrations and sensor offset, an adaptive Smith predictor controller was implemented using the developed algebraic estimators. A fractional-order derivative controller has been embedded in the Smith predictor structure in order to remove the steady-state error caused by the strain gauge offset. These algorithms have been validated in an experimental platform. This controller adapts its parameters faster and in a more effective manner than what has been achieved to date.

ACKNOWLEDGMENT

This research was funded in part by the Grant PID2022-141409OB-C21 funded by MCIN/AEI/ 10.13039/ 501100011033 / FEDER "A way of making Europe" and in part by the University of Castilla-La Mancha (Spain) and the European Social Fund (FEDER) under Project 2023-GRIN-34307.

REFERENCES

[1] Neal Y Lii, Zhaopeng Chen, Benedikt Pleintinger, Christoph H Borst, Gerd Hirzinger, and Andre Schiele. Toward understanding the effects of visual-and force-feedback on robotic hand grasping performance for space teleoperation. In *2010 IEEE/RSJ International Conference on Intelligent Robots and Systems*, pages 3745–3752. IEEE, 2010.

[2] Mohadeseh Yaryan, Mahyar Naraghi, Seyed Mehdi Rezaei, Mohammad Zareinejad, and Hamed Ghafarirad. Bilateral nonlinear teleoperation for flexible link surgical robot with vibration control. In *2012 19th Iranian conference of biomedical engineering (ICBME)*, pages 101–106. IEEE, 2012.

[3] Olatunji Mumini Omisore, Shipeng Han, Jing Xiong, Hui Li, Zheng Li, and Lei Wang. A review on flexible robotic systems for minimally invasive surgery. *IEEE Transactions on Systems, Man, and Cybernetics: Systems*, 52(1):631–644, 2020.

[4] Han Wang, Hongling Sun, Yunping Sun, Ming Wu, and Jun Yang. A narrowband active noise control system with a frequency estimation algorithm based on parallel adaptive notch filter. *Signal Processing*, 154:108–119, 2019.

[5] Ting Cui, Feng Ding, Xiangli Li, and Tasawar Hayat. Kalman filtering based gradient estimation algorithms for observer canonical state-space systems with moving average noises. *Journal of the Franklin Institute*, 356(10):5485–5502, 2019.

[6] Erick F Alves, Jonas K Nϕland, Giancarlo Marafioti, and Geir Mathisen. Online parameter identification of synchronous machines using kalman filter and recursive least squares. In *IECON 2019-45th Annual Conference of the IEEE Industrial Electronics Society*, volume 1, pages 7121–7128. IEEE, 2019.

[7] Yang Deng, Vincent Léchappé, Sébastien Rouquet, Emmanuel Moulay, and Franck Plestan. A practical online time-varying delay estimation of remote control system based on adaptive super-twisting algorithm. In *2020 IEEE Conference on Control Technology and Applications (CCTA)*, pages 885–891. IEEE, 2020.

[8] Abdelbacet Mhamdi, Kaouther Ibn Taarit, and Moufida Ksouri. Online algebraic identification approach of continuous linear time delay systems. *Asian Journal of Control*, 20(1):343–355, 2018.

[9] Lotfi Belkoura. Identifiability and algebraic identification of time delay systems. *IFAC Proceedings Volumes*, 43(2):1–8, 2010.

[10] Juan R Trapero, Hebertt Sira-Ramírez, and Vicente Feliu Batlle. An algebraic frequency estimator for a biased and noisy sinusoidal signal. *Signal processing*, 87(6):1188–1201, 2007.

[11] Michel Fliess and Hebertt Sira-Ramírez. An algebraic framework for linear identification. *ESAIM: Control, Optimisation and Calculus of Variations*, 9:151–168, 2003.

[12] Claudia F Yaşar. Algebraic estimator of parkinson's tremor frequency from biased and noisy sinusoidal signals. *Transactions of the Institute of Measurement and Control*, 43(3):679–686, 2021.

[13] Juan R Trapero, Hebertt Sira-Ramírez, and Vicente Feliu Batlle. A fast on-line frequency estimator of lightly damped vibrations in flexible structures. *Journal of Sound and Vibration*, 307(1-2):365–378, 2007.

[14] Selma Benftima, Vicente Feliu Batlle, Selma Benattia, and Salah Salhi. A fast online estimator of the main vibration mode of mechanisms from a biased slightly damped signal. In *IECON 2022–48th Annual Conference of the IEEE Industrial Electronics Society*, pages 1–6. IEEE, 2022.

[15] Andres San-Millan and Vicente Feliu. A fast online estimator of the two main vibration modes of flexible structures from biased and noisy measurements. *IEEE/ASME Transactions on Mechatronics*, 20(1):93–104, 2014.

[16] Sana Baklouti, Guillaume Gallot, Julien Viaud, and Kevin Subrin. On the improvement of ros-based control for teleoperated yaskawa robots. *Applied Sciences*, 11(16):7190, 2021.

[17] S Farokh Atashzar, Mahya Shahbazi, Heidar A Talebi, and Rajni V Patel. Control of time-delayed telerobotic systems with flexible-link slave manipulators. In *2012 IEEE/RSJ International Conference on Intelligent Robots and Systems*, pages 3035–3040. IEEE, 2012.

[18] Padideh Rasouli, Ahmad Forouzantabar, Mazda Moattari, and Mohammad Azadi. Fault-tolerant control of teleoperation systems with flexible-link slave robot and disturbance compensation. *Iranian Journal of Science and Technology, Transactions of Electrical Engineering*, 44:1487–1499, 2020.

[19] Emmanuel Nuño, Ioannis Sarras, Luis Basañez, and Michel Kinnaert. Control of teleoperators with joint flexibility, uncertain parameters and time-delays. *Robotics and autonomous systems*, 62(12):1691–1701, 2014.

[20] V Feliu-Batlle. Robust isophase margin control of oscillatory systems with large uncertainties in their parameters: A fractional-order control approach. *International Journal of Robust and Nonlinear Control*, 27(12):2145–2164, 2017.